

# A Stationary CT Scheme Based on Field Emission Flat-panel X-ray Source Array

Haitao Cheng, Kai Wang, and Xuanqin Mou

**Abstract**—With the development of field emission x-ray cold cathodes of nanomaterials, several new x-ray imaging geometries have been proposed. Compared with thermionic x-ray tube, this new type of x-ray tube is of great advantages, such as fast response, low energy consumption and individually addressable switching. In this work, a new tomographic geometry is devised, in which a stationary polygon-shape flat-panel cathode source array is employed to avoid mechanical movement for scanning. With an array of sources implemented in a flat-panel, each source irradiates a narrow cone beam x-ray and all the beams from the panel are overlapped to cover the scanned object. A number of the flat-panels, as well as x-ray detectors of the same number, are grouped as a polygon that encloses the object to implement a rotation-free projection acquisition. With the proposed geometry, we experimentally explore two scanning schemes, i.e., switching source separately or simultaneously. Numerical experiments demonstrated that in separating switching, low root mean square error and high contrast to noise ratio is achieved with more sources distributed in the flat-panel. For simultaneous switching, image quality is restricted by few-view nature and overlapping projection. With the limitation of constant current power and x-ray dose, the scheme of  $10 \times 10$  sources distributed in the flat-panel can produce an advisable reconstruction result.

**Index Terms**—field emission cathode, flat-panel x-ray sources, iterative reconstruction

## I. INTRODUCTION

In recent years, the development of field emission cathode offers new opportunities in developing new x-ray imaging mechanisms due to the inherent superiorities of the new type of cathode, such as stable radiation, controllable emission field, fast response time, and low emission threshold potentials [1][2]. At the same time, field emission cold cathodes, e.g., carbon nanotube(CNT), allow the possibility of programmable x-ray source multiplexing in design of scanning modality [3][4]. The application of cold cathode makes it easier to pack multi-source closely together, such x-ray source array allows rapid tomographic imaging without motion blur, by fast switching sources in series rather than rotating or translating a single source. This novel characteristic of the array source gives motivation of proposing different geometric schemes with the x-ray source array to solve existing problems in conventional computed tomography(CT).

This work was supported in part by the National Key Research and Development Program of China (No. 2016YFA0202003) and the National Natural Science Foundation of China (No. 61401349, No.61571359).

The authors are with the Department of the Institute of Image Processing and Pattern Recognition, Xi'an Jiaotong University, Xi'an, Shaanxi 710049, China

In the flat panel imaging field, G. Yang et al. utilized multi-beam field emission x-ray source array to design tomosynthesis system for the total imaging time reduction, simplifying the system design, and potentially improving the image quality [5]. Z. Zhang et al. used surrounding x-ray sources and flat-panel detectors to collect projection data with few angle rotations [6]. E. Quan et al. proposed a rotation-free micro-CT system with square and hexagonal geometries, which utilize individual characters of CNT to switch source one by one [7].

In our study, we propose a new stationary CT geometry based on the field emission flat-panel x-ray sources of diode structure using ZnO nanowires as cold electron emitters [8]. And polygon-shape flat-panel x-ray source array is employed to avoid rotation in the system, where every source irradiates a narrow cone beam x-ray and all the beams from the panel are overlapped to cover the whole 3D object. With several sources integrated in a flat-panel, the distance between x-ray sources and object can be closer, and the design of source upside and detector downside ensures more projections and free-rotation. 2D source array and oblique emission are used to cover more regions of object. Specially, we make use of constant small cone angle with uniform lead collimator to guarantee the uniform distribution of x-ray radiation, in consideration of constant current power and x-ray dose, this is, in the situation of constant total photon number, more sources mean more quantum noise, we study associated reconstruction algorithm and optimized sources distribution to provide the reference for the design of flat-panel x-ray source array.

## II. METHODS

### A. System Description

The whole system geometry is composed of multiple plates of x-ray sources array in upside and the detector area in downside, as shown in Fig.1. And each source irradiates a narrow cone beam x-ray with same small cone angle of  $7^\circ$  and emission direction toward opposite oblique downside detector. In the meantime, every source just irradiates certain region of object under scanned, and all the beams from the panel are overlapped to cover the whole object.

Suppose there are  $m$  planes to enclose the object with  $n \times n$  x-ray source implemented in a flat-panel. To obtain the object internal tomographic information, two different scanning schemes are designed.

The first one is to make use of individual addressable character and ultra-switch time of field emission cathode x-ray

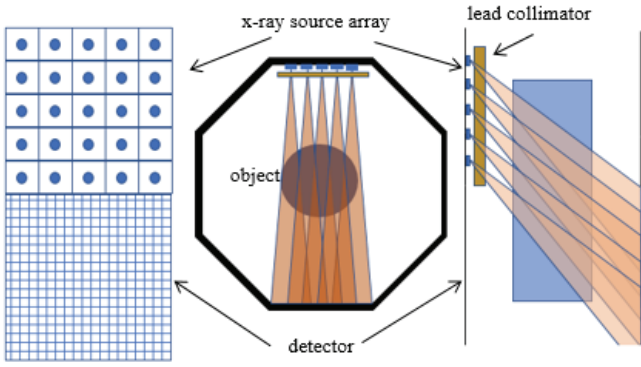


Fig. 1. system design scheme of stationary CT based on field emission x-ray source array. The integration of same-size x-ray source array and detectors (left), an octagon embrace (middle), and cone beam emission from one source array at one time(right).

source to flash every source individually in order to obtain a number of same-size projection images, as well as x-ray sources of the same number, as shown in Fig.2(a). And every source interacts with the little regions of object and produces a circular bright spot projection in opposite oblique downside detector area, as shown in Fig.2(d); another equivalent choice is to make all sources divided into several groups as small as possible, but there are not intersected sections in projection data when flash all sources in any group, as shown in Fig.2(b). And we get some same-size projection images, as well as x-ray sources groups of the same number, and the several bright spots are observed in projections, as shown in Fig.2(e). Compared with the previous one, this method can decrease the scanning time. Actually, the two strategies are same and interconvertible in mathematics, so we call the two methods as separating switching. The second scheme is to flash all x-ray sources in a flat-panel every time, we can get several projection images whose number is equal with the number of source array, as shown in Fig.2(c). Compared with separating switching, this method (simultaneous switching) can decrease emission duration, but there are many intersected sections in detector projections which are composed of many bright spots and bring in overlapping problem in projection images, as shown in Fig.2(f).

### B. Forward projection model

In conventional x-ray emission, the measured photon counts in  $p$ -th detector unit can be written as:

$$\hat{y}_p = I_{pq} \exp(-a_{pq}x) + n_p \quad (1)$$

where  $I_{pq}$  are the emission counts from  $q$ -th ( $q = 1, \dots, Q$ ) source to opposite  $p$ -th ( $p = 1, \dots, P$ ) detector,  $P$  is the number of detector units and  $Q$  is the number of array sources in source-detector pair,  $\hat{y}_p$  is the expected measurement of response photon number in  $p$ -th detector,  $a_{pq}$  is the length along the x-ray path,  $x$  is the object attenuation coefficient and  $n_p$  is the random noise. Note that multi-source situation in our proposed system frame, we modify Eq.(1) as:

$$\hat{y}_p = \sum_{q=1}^Q I_{pq} \exp(-a_{pq}x) + n_p \quad (2)$$

where  $Q$  is the number of source at one time. Actually, multi-source emission means that real measurement  $\hat{y}_p$  is the sum of individual source emission.

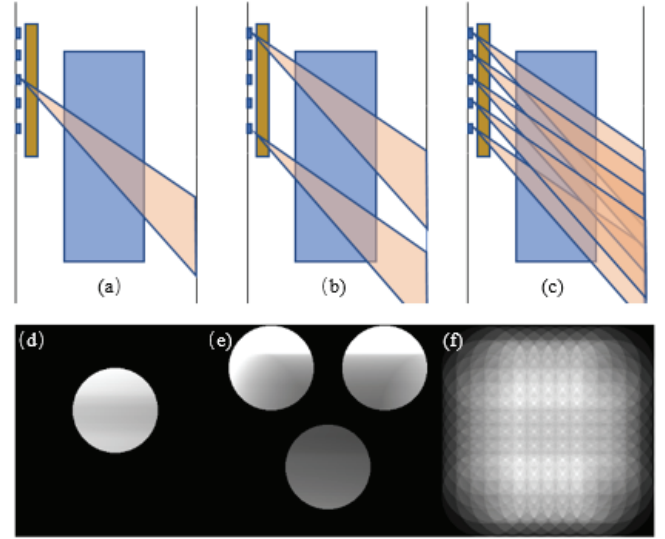


Fig.2. projections in two different schemes, In separating switching scheme(a)(b), (d)and(e) are associated projection data for switching 44th source or switching 10th ,48th and 81st sources. For simultaneous switching scheme (c), (f) is corresponding projection for switching all 100 sources in one plane.

### C. Reconstruction Algorithm

To obtain the internal structure for diagnostics or evaluation with the projection data from the geometry, a reconstruction algorithm is proposed.

The cost function in image reconstruction is :

$$\min_x \sum_{p=1}^{mP} \left\| \sum_{q=1}^Q I_{pq} \exp(-a_{pq}x) - \hat{y}_p \right\|_2^2 + \beta R(x) \quad (3)$$

The first term indicates the data fidelity in the L2-norm. The second term consists of  $R(x)$  as a regularization function. For example, the total variation(TV) norm is a popular regularization choice for sparsity-based CT image reconstruction [9].

Note that Eq.(3) could be written as followed when every detector response comes from single source:

$$\min_x \sum_{p=1}^{mP} \sum_{q=1}^Q \left\| I_{pq} \exp(-a_{pq}x) - \hat{y}_p \right\|_2^2 + \beta R(x) \quad (4)$$

The reconstruction algorithm for Eq.(4) is equivalent to conventional CT by logarithmic operation:

$$\min_x \sum_{p=1}^{mP} \sum_{q=1}^Q \left\| a_{pq}x - \hat{b}_p \right\|_2^2 + \beta R(x) \quad (5)$$

where  $\hat{b}_p = \log \frac{I_{pq}}{\hat{y}_p}$  represents the linear integral value along the x-ray path from  $q$ -th source to opposite  $p$ -th detector.

For the situation that multi x-ray sources emit photons toward one detector unit, one particular algorithm is proposed for Eq.(4).

In  $p$ -th detector for simultaneous switching, the residual error is:

$$d_p = \left( \hat{y}_p - \sum_{q=1}^Q I_{pq} \exp(-a_{pq}x) \right)^2 \quad (6)$$

Respectively, the first derivative and the second-order derivative are calculated:

$$\frac{d(d_p)}{dx} = 2 \sum_{i=1}^Q I_{pi} a_{pi} \exp(-a_{pi}x) * \left( \sum_{q=1}^Q I_{pq} \exp(-a_{pq}x) - \hat{y}_p \right) \quad (7)$$

$$\frac{d^2(d_p)}{dx^2} = \sum_{i=1}^Q I_{pi} \|a_{pi}\|^2 \exp(-a_{pi}x) * \left( \sum_{q=1}^Q I_{pq} \exp(-a_{pq}x) - \hat{y}_p \right) + \left( \sum_{i=1}^Q I_{pi} \|a_{pi}\| \exp(-a_{pi}x) \right)^2 \quad (8)$$

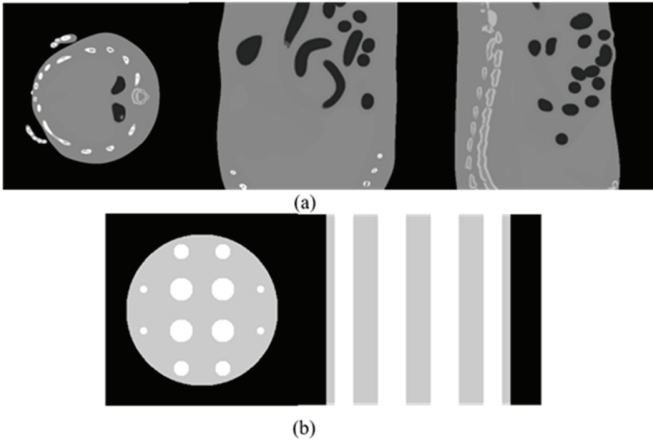


Fig.3. two phantoms used in the simulations (a)The chosen coronal (left), sagittal (middle), and transaxial (right) views of the MOBY mouse phantom(b) The central coronal (left), profile(right) view from the designed column phantom.

we conduct the reconstruction by using Newton's method for convex optimization, and the update equations are as follows:

$$x_{n+1} = x_n - \lambda \frac{\sum_{p=1}^{mP} \frac{d(d_p)}{dx}}{\sum_{p=1}^{mP} \frac{d(d_p)^2}{dx^2}} \quad (9)$$

where  $\lambda$  is relaxation factor. And we obtain the reconstruction results by iteration.

### III. EXPERIMENT

#### A. Numerical Simulation

In the numerical simulation, two phantoms were used as shown in Fig.3. And all x-ray sources were monochromatic and detectors were considered ideal. The distance between source plane and detector plane is 12 cm. A total  $5 \times 5$ ,  $10 \times 10$  and  $20 \times 20$  sources equidistantly distributed in a flat-panel, corresponding distance among all x-ray sources is 10mm, 5mm, and 2.5mm. And projection data of the phantoms was generated on eight detector area, where detector pixel is  $200 \times 200$  with a resolution of  $0.25 \text{ mm} \times 0.25 \text{ mm}$ . Besides, more Poisson noise is added with more sources in consideration of the constant power, in each case, 16, 4,  $1(\times 10^3)$  photons per detector-source pair are used to guarantee constant total photon number.

Two phantoms are used and the first phantom is MOBY which it is a NURBS-defined realistic mouse phantom [10], as shown in Fig.3(a). The second is our designed column phantom which is comprised of the round background in the diameter of 50mm and three kinds of round in the diameter of 2.5mm, 5mm and 7.5mm. as shown in Fig.3(b).

We employ TV constraints on the attenuation coefficient to perform sparsity regularization in the attenuation coefficient gradient as penalty term. On the other hand, we use the gradient as penalty term. On the other hand, we use the Nesterov's acceleration algorithm to boost convergence [11]. And during the reconstructions, we use 200 iterations and 2 ordered subsets [12]. And the size of reconstructed images is set to  $256 \times 256 \times 200$  with a voxel size of  $0.25 \times 0.25 \times 0.25 \text{ mm}^3$  in our experiments.

Finally, we measure the convergence rate of the two different scanning schemes and use the root mean square errors (RMSE)

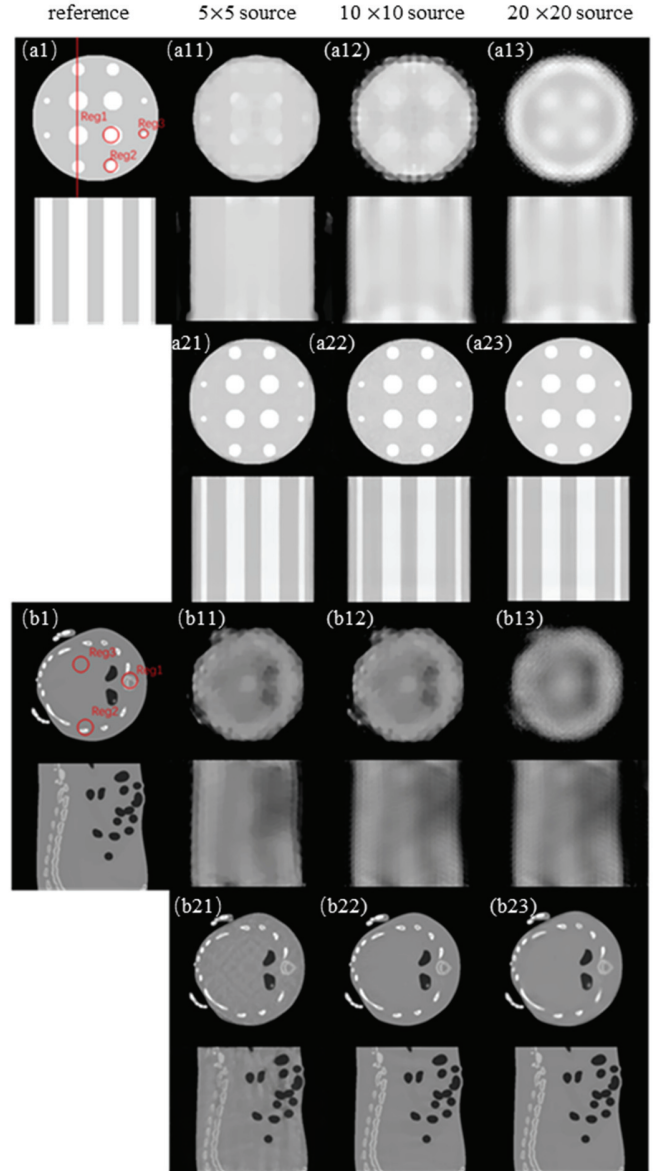


Fig.4. reference images and reconstruction results. (a1)is coronal and profile(red line ) reference image for column phantom and three ROIs. (a11) (a12) and (a13) are reconstruction for  $5 \times 5$ ,  $10 \times 10$ ,  $20 \times 20$  by simultaneous switching((a21) (a22) and (a23) are reconstruction by separating switching. (b1)is reference image for MOBY phantom and three ROIs. (b11) (b12) and (b13) are reconstruction for  $5 \times 5$ ,  $10 \times 10$ ,  $20 \times 20$  by simultaneous switching((b21) (b22) and (b23) are reconstruction by separating switching.

and contrast to noise ratio(CNR) to evaluate our reconstruction results in a chosen coronal. We measure the CNR in three same-size regions in MOBY phantom, where there exist bones and smooth tissue respectively, as shown in Fig.4(a1). And three different size regions are observed, corresponding three spots in the simple phantom, as shown in Fig.4(b1). The size of background region is chosen as the twice than size of ROIs.

#### B. Results

We present several experiment results in different scanning schemes and phantoms, as shown in Fig.4, and we measure the RMSE and CNR for images by switching separately, as shown

TABLE 1  
CNR OF FIG. 4. REPRESENTATIVE ROIs AND RMSE MEASUREMENT FOR SEPERATING SWITCHING

source array	column phantom				MOBY phantom			
	CNR			RMSE(unit $cm^{-1}$ )	CNR			RMSE(unit $cm^{-1}$ )
	region1	region2	region3		region1	region2	region3	
5×5	4.0836	1.8268	0.5217	0.00908	0.2991	0.8236	0.0377	0.01812
10×10	4.2609	2.0567	0.6258	0.00744	0.2814	0.8764	0.0089	0.00718
20×20	4.2432	1.9276	0.5190	0.00729	0.2978	0.8787	0.0078	0.00709

in Table 1.

For switching simultaneously, the reconstruction results are good enough whether column phantom or MOBY phantom is used, as shown in Fig.4(a21)-(a23) and Fig.4(b21)-(b23). And the lower RMSE and higher CNR are achieved while the number of sources distributed in flat-panel is increasing. The image qualities are improved much from 5×5 sources array to 10×0 sources array but little to 20×20 sources array. Note that in the region3 of MOBY phantom, results for 5×5 sources array could have higher CNR because high noise in smooth region.

For column phantom when switching simultaneously, there is local diffusion by 5×5 sources array, as shown in Fig.4(a11). Block artifacts exist in image by 10×10 sources array, where the noise could not be suppressed easily, as shown in Fig.4(a12). And ring artifacts of images by 20×20 sources array have many effects in edge, where small spot signals are covered, as shown in Fig.4(a13).

When all sources are switched simultaneously, the reconstruction images of the MOBY phantom, whose structure is more complex, are not good enough, as shown in Fig.4(b11)-(b13). All results have some blurred octagonal border, and internal structure is vague, tissues and bones are difficult to distinguish.

### C. Discussion

In general, the reconstruction results by separating switching are better than results by simultaneous switching. The major reason is that few projections generated by simultaneous switching could not offer more information and confusion from overlapped projection produce some block artifacts by iterative penetration.

Respectively, the reconstruction results are closely to the ground truth by separating switching, but when switching sources simultaneously, the reconstruction results for designed phantom are not good and results for MOBY phantom are worse that all detailed structures could not be observed from reconstruction results because of sparse-view problem. With more sources distributed in flat-panel, overlapping projections are more serious, which results that block artifacts are brought in reconstruction images by back projection of intersection projected portion.

On the other hand, in the simulation experiments, more noise with more sources distributed in a flat-panel could have little effects with the reconstruction results, that is, more projection data is useful for reconstruction in spite of more noise existing in data. But considering that the size of source focal spot could

not be neglected and RMSE is little decreased with denser sources, 10×10 sources array could be a good choice.

## IV. CONCLUSION

In this paper, we proposed a novel flat-panel x-ray source imaging scheme, deduced the forward model and the reconstruction algorithm. Meanwhile, we experimentally investigated two scanning strategies. When switching separately in scanning, there would be less artifacts, lower RMSE, higher CNR and better image qualities with more sources distributed in flat-panel. For simultaneous switching, the image qualities are restricted by the few-angle and overlapping projections. According to the experimental result, we suggested the 10×10 source array scheme as reference for our future work.

## REFERENCES

- [1] Li Y, Sun Y, Yeow J T W. Nanotube field electron emission: principles, development, and applications[J]. *Nanotechnology*, 2015, 26(24): 242001.
- [2] Baughman R H, Zakhidov A A, de Heer W A. Carbon nanotubes--the route toward applications[J]. *science*, 2002, 297(5582): 787-792.
- [3] Zhang J, Yang G, Cheng Y, et al. Stationary scanning x-ray source based on carbon nanotube field emitters[J]. *Applied Physics Letters*, 2005, 86(18): 184104.
- [4] Zhang J, Cheng Y, Lee Y Z, et al. A nanotube-based field emission x-ray source for microcomputed tomography[J]. *Review of scientific instruments*, 2005, 76(9): 094301.
- [5] Yang G, Rajaram R, Cao G, et al. Stationary digital breast tomosynthesis system with a multi-beam field emission x-ray source array[C]. *Medical Imaging. International Society for Optics and Photonics*, 2008: 69131A-69131A-10.
- [6] Quan E M, Lalush D S. Three-dimensional imaging properties of rotation-free square and hexagonal micro-CT systems[J]. *IEEE transactions on medical imaging*, 2010, 29(3): 916-923.
- [7] Zhang Z, Yu S, Liang X, et al. A novel design of ultrafast micro-CT system based on carbon nanotube: A feasibility study in phantom[J]. *Physica Medica*, 2016, 32(10): 1302-1307.
- [8] Chen D, Song X, Zhang Z, et al. Transmission type flat-panel X-ray source using ZnO nanowire field emitters[J]. *Applied Physics Letters*, 2015, 107(24): 243105.
- [9] Sidky E Y, Kao C M, Pan X. Accurate image reconstruction from few-views and limited-angle data in divergent-beam CT[J]. *Journal of X-ray Science and Technology*, 2006, 14(2): 119-139.
- [10] Segars W P, Tsui B M W, Frey E C, et al. Development of a 4-D digital mouse phantom for molecular imaging research[J]. *Molecular Imaging & Biology*, 2004, 6(3): 149-159.
- [11] Kim D, Ramani S, Fessler J A. Accelerating X-ray CT ordered subsets image reconstruction with Nesterov's first-order methods[C]. *Proc. Intl. Mtg. on Fully 3D Image Recon. in Rad. and Nuc. Med.* 2013: 22-5.
- [12] Wang G, Jiang M. Ordered-subset simultaneous algebraic reconstruction techniques (OS-SART)[J]. *Journal of X-ray Science and Technology*, 2004, 12(3): 169-177.